Journal of Material Science and Mechanical Engineering (JMSME)
p-ISSN: 2393-9095; e-ISSN: 2393-9109; Volume 3, Issue 3; April-June, 2016 pp. 172-178

http://www.krishisanskriti.org/Publication.html

Heat Transfer Enhancement from a Ribbed Surface in Presence of a Cross Flow Jet: A Numerical Investigation

Arnab Mukherjee[1], Swetapadma Rout[2] and Ashok K. Barik[3]

[1,2,3]Mechanical Engineering Department, College of Engineering and Technology, Bhubaneswar
E-mail: [3]ashokbarik.mech@gmail.com

Abstract—*In the present study, a rectangular channel with different protruded surfaces is investigated numerically in a three–dimensional computational domain. Two different protrusion shapes have been tested trapezoidal and triangular. A finite volume technique has been used to solve the conservation equations for mass, momentum, and turbulence (SST $k-\omega$ turbulence). The duct Reynolds numbers are varied in the range of* $18,263 \leq Re_{Dh,duct} \leq 54,789$. *An impinging jet normal to the main flow has been deployed to study its effect on heat transfer enhancement. The heat transfer enhancements with and without cross-flow effects have been compared. It has been observed that the heat transfer rate with cross-flow effect is higher that the non-cross-flow effect. The thermo-hydraulic characteristics of the mean flow due the cross-flow and non-cross flow effects have also been discussed. It is also observed that the geometrical shape of the protrusion have a significant effect on the heat transfer augmentation. The heat transfer enhancement with triangular protrusions is found to be more compared to the other protrusion shapes. The inter-protrusion flow recirculation in the context of heat transfer enhancement has also been discussed.*

1. INTRODUCTION

The demand for an effective method of the heat elimination from an electronic device is growing at a rapid rate owing to the miniaturization of electronics device, higher power density and higher operational speed. Simple forced convective heat transfer method may not be sufficient enough to dissipate heat so as to safeguard the electronic components. A hybrid cooling strategy which utilizes the benefits of heat transfer enhancement by forced convection, jet impingement as well as surface protrusions has been proposed in the present study.

A comprehensive study has been carried out by Mudawar [1] and Yeh [2] employing different cooling techniques for electronic devices. Heat transfer from the hot wall can be enhanced by putting turbulators of various shapes such as transverse ribs [3-4], W- shaped ribs [5], and V-shaped ribs [6]. Also the perforations in the ribs can enhance heat transfer rate significantly by breaking the viscous sub-layer near the wall, which leads to a higher mixing rate of fluids. The heat transfer enhancement for full and half perforated baffles attached to a hot surface was studied by Karwa et al. [7] and Karwa and Maheshwari [8]. The thermo hydraulic performance of a turbulent flow through a tube fitted with perforated tube inserts have been investigated by Bhuiya et al [9]. In an experimental study, Alam et al. [10] reported that Nusselt number for a perforated V-shaped blockage has been improved by 33% as compared to a solid blockage. Heat transfer enhancement using ribs of different shapes (such as rectangular, trapezoidal and delta) has also been investigated by Zhou and Feng [11].

It was shown by various researchers [12-14] that the heat transfer augmentation by jet impingement is one of the efficient methods which can dissipate heat more effectively compared to a simple forced convection method.

Moreover, further heat transfer augmentation can be achieved by a hybrid method in an impinging jet is deployed normal to main flow. A hybrid heat transfer augmentation method has been adopted by Tan et al. [15] by impinging air jet on a protruded surface. Two different (i.e., V and rectangular) shapes of protrusions have been employed by them to investigate the heat transfer rate in the Reynolds number range of 6,000 to 30,000. For same jet Reynolds number, the heat transfer was augmented by 30% when a smooth wall was replaced by a ribbed wall. In another attempt, different cross flow schemes for micro grooved surface were investigated by Xing et al. [16]. The best heat transfer performance was attained at the minimum cross flow as had been demonstrated by them. A similar study was conducted by Su and Chang [17] to study the combined effects of groove and nozzle size distribution on heat transfer enhancement. Liquid Crystal Thermography (LCT) had been implemented by Wang et al. [18] to investigate heat transfer in cross flow. They reported that a more pronounced effect on heat transfer enhancement was found out at a lower velocity ratio. A flow visualization methods had been carried out by Nakabe et al. [19] by using an inclined impinging jet in a cross flow.

It is clear from the above literature review that the research on the heat transfer augmentation in the presence of a cross flow jet is still in infant stage. Thus, the heat transfer augmentation in the presence of the cross flow jet has been studied numerically in the present investigation by varying different pertinent operating parameters such as duct and nozzle Reynolds number. A comparison for the heat transfer enhancement has been shown for a cross flow and non-cross flow arrangement.

2. MATHEMATICAL FORMULATION

2.1 Physical Description and Grid Arrangement

In the present numerical investigation, a rectangular duct of size 0.67 m × 0.023 m × 0.03 m has been used as shown in Fig. 1. Air enters the inlet of the rectangular duct at velocity and temperature of u_{in} and T_∞, respectively. Also, air is impinged normal to the main flow by placing a square nozzle on the top surfaces of the duct so that they will form a cross flow with each other. This will enhance the mixing and hence, increases the heat transfer rate from the bottom hot surface. Moreover, protrusions of different shapes (i.e., trapezoidal and triangular) have also been provided on the bottom hot surface to further augment the heat transfer rate. The hot surface (of length $X / Dh_{duct} = 5.76$) is maintained at a constant temperature (T_w). An extra length of 10 times the hydraulic diameter of the duct has been considered so as to ensure a fully developed flow in the duct.

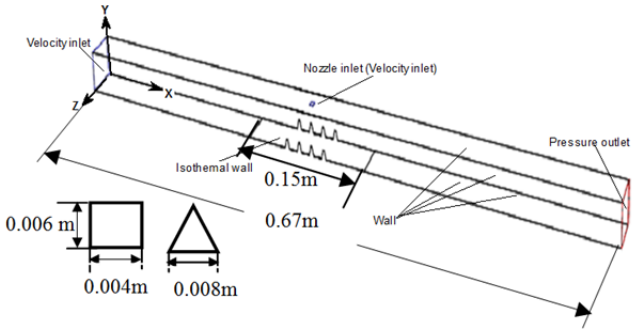

Fig. 1: Schematic diagram of computaional domain with diffrent boundary conditions and different potrusions

Similarly, an extra length of 10 times the hydraulic diameter is taken in downstream of the hot surface to reduce the effect of backflow at the exit.

The inlet surfaces as well as the outlet surfaces are meshed with triangular cells. The bottom surface except the hot wall is meshed with rectangular cells in order to control the number of cells. Tetrahedral meshes have been adopted to mesh the hot surface along with the protrusions. Therefore, the total computational domain is meshed with a hybrid meshing scheme (i.e., combination of hexahedral and tetrahedral meshes). The hydraulic diameter of the nozzle is 0.005 m.

Following assumptions are taken for solving the governing equations:

1. The working fluid (air) is Newtonian and incompressible.
2. Flow is steady, three-dimensional and turbulent.
3. Fluid properties such as thermal conductivity (λ), dynamic viscosity (μ), and specific heat (c_p) are kept constant.

2.2 Governing Equations

The Reynolds time-averaged equations for mass, momentum, energy in an inertial reference frame are written as follows:

Continuity equation: $$\frac{\partial \overline{u_i}}{\partial x_i} = 0 \quad (1)$$

Momentum equation: $$\rho \overline{u_i} \frac{\partial \overline{u_i}}{\partial x_i} = -\frac{\partial \overline{p}}{\partial x_i} + \frac{\partial}{\partial x_j}\left(2\mu \overline{S_{ij}} - \rho \overline{u_i' u_j'}\right) \quad (2)$$

Energy equation: $$\rho \overline{u_j} \frac{\partial \overline{T}}{\partial x_j} = \frac{\partial}{\partial x_j}\left(\frac{\lambda}{c_p}\frac{\partial \overline{T}}{\partial x_i} - \rho \overline{u_i' T'}\right) \quad (3)$$

The mean stain rate is defined as:

$$\overline{S_{ij}} = \frac{1}{2}\left(\frac{\partial u_i}{\partial x_j} + \frac{\partial u_j}{\partial x_i}\right) \quad (4)$$

Where μ, λ and c_p represent the dynamic viscosity, thermal conductivity and specific heat at constant pressure for the working fluid, respectively. The Reynolds stress ($-\rho \overline{u_i' u_j'}$) and turbulent heat flux ($-\rho \overline{u_i' T'}$) terms are appearing due to the time averaging, and these terms need to be closed by using the appropriate turbulence model. The Reynolds stress can be specified using a linear eddy viscosity model as follows:

$$-\rho \overline{u_i' u_j'} = 2\mu_t \overline{S_{ij}} - \frac{2}{3}\rho k \delta_{ij} \quad (5)$$

Where, k denotes the turbulent kinetic energy and μ_t represents the eddy viscosity, which are to be specified by solving the transport equations for the turbulent kinetic energy (k) and specific dissipation rate using the $k-\omega$ turbulence model. Similarly, the turbulent heat flux is defined as

$$-\rho \overline{u_i' T'} = \frac{\mu_t}{Pr_t}\frac{\partial \overline{T}}{\partial x_i} \quad (6)$$

Here, Pr_t denotes the turbulent Prandtl number. The SST $k-\omega$ turbulence model proposed by Mentor [20] is implemented in the present study so as to model the turbulence quantities. The governing equations for the turbulence kinetic energy (k) and specific dissipation of turbulence kinetic energy (ω) can be seen from Ref. [21]

Different model constants used in SST $k-\omega$ turbulence model are given as follows [21]:

$\alpha_{\infty}^{*}=1, \beta_{\infty}^{*}=0.09, \beta_i=0.072, \sigma_{k,1}=1.176\ \sigma_{\omega,1}=2, \sigma_{k,2}=1,$
$\sigma_{\omega,2}=1.168, R_k=6, a_1=0.31$ and $R_{\beta}=8.$

2.3 Boundary conditions

The applied boundary conditions for present the computational domain has been shown in Fig. 1. The velocity inlet boundary conditions have been imposed on nozzle and duct inlets, as air enters the computational domain through these surfaces. The side and top surfaces (excluding the nozzle inlet) are taken as adiabatic wall. A constant temperature has been imposed to the isothermal wall. The pressure outlet boundary condition is applied to outlet because the ambient pressure is prevailed there.

The mathematical descriptions of different boundary conditions are given as follows:

At adiabatic walls:

$$u=v=w=0, \text{ and } \frac{\partial T}{\partial x}=\frac{\partial T}{\partial y}=\frac{\partial T}{\partial z}=0 \quad (7)$$

At solid isothermal wall:

$$u=v=w=0, \text{ and } T=T_w \quad (8)$$

At duct inlet: $u_p=u_{in}, T=T_{\infty}$ (9)

At nozzle inlet: $v=-v_{in}, T=T_{\infty}$ (10)

Here u, v and w are the velocity components in the x, y, and z- direction, respectively.

At pressure outlet: $p=p_{\infty}$ and $T=T_{\infty}$ (11)

Where, p_{∞} and T_{∞} are the ambient pressure and temperature, respectively. The standrad wall function as proposed by Launder and Spalding [22] has been used to link the solution variables at near-wall cells to the corrsponding quantitites on the wall. Similar wall functions have been epmloyed by Jha and Dash [23]and Barik et al. [24-25]. The law-of-wall for mean velocity is given as:

$$\frac{\rho u_p k_p^{1/2} c_{\mu}^{1/4}}{\tau_w/\rho}=\frac{1}{\kappa}\ln\left(E y^{*}\right) \quad (12)$$

$$y^{*}=\frac{\rho k_p^{1/2} c_{\mu}^{1/4} y_p}{\mu} \quad (13)$$

Where, *E* denotes the emperical constant equal to 0.793, κ is the von Karman constant having a value 0.4187 and u_p is the mean velocity of fluid at a point *'p'*. The turbulent intensity at duct and nozzle inlets are computed as $I=0.016Re^{-1/8}$ (14)

2.4 Numerical solution procedure

The governing equations for mass, momentum, energy, turbulent kinetic energy (k) and the specific dissipation (ω) are discretized in a three-dimensional computational domain to yield a set of algebraic equations, which are then solved by imposing the boundary conditions with the second order upwind scheme of Ansys-Fluent 16.0. SIMPLE algorithm has been employed for pressure- velocity coupling to solve pressure correction equation. In the present study, the SST $k-\omega$ turbulence model has been used. In the past, it was recommended by various researchers [26-27] to use SST $k-\omega$ model. They concluded that both standard as well as SST $k-\omega$ models were capable of predicting the surface Nusselt number very well, when the ratio of the jet spacing to the hydraulic diameter of the nozzle was low (i.e., 4 to 4.9). In the present study, this ratio is kept at 4.6. Thus, it is expected that SST $k-\omega$ model may predict the heat transfer quite well.

3. VALIDATION OF NUMERICAL METHODOLOGY"

The present numerical scheme has been validated with some of the existing experimental data available in the literature. However, the heat transfer augmentation and thermal management of a mini rectangular channel with surface protrusions and the cross flow approach is a new research area. Hence, the literature on such a hybrid cooling scheme is sparse. Nevertheless, the present numerical scheme is validated with Sleicher and Rouse [28] correlation by taking a three-dimensional circular pipe of diameter 0.026 m and length 0.67 m, and applying a uniform wall heat flux (i.e. 100 W/m^2) to the fully developed portion of the duct. This particular problem is chosen, since the boundary conditions for the validation purpose is similar with our present boundary conditions.

A grid sensitivity test has also been carried out for the present validation, and it is found that a grid size of 28,891 cells predicted the surface Nusselt number reasonably well with the above correlation as shown in Fig. 2. However, the Sielder and Tate [29] correlation over predicts the Nusselt number since it is used for the fluids having a temperature dependent properties. Moreover, the computed values of Nusselt number are closer to the values predicted by Kakac et al. [30] correlation. For the above validation, SIMPLE method has been used for pressure-velocity coupling and the second order upwind scheme is used for solving mass, momentum and energy equations. SST $k-\omega$ model has been used for the simulation. From this discussion, it is clear that the present numerical scheme is capable of predicting the surface Nusselt number very well.

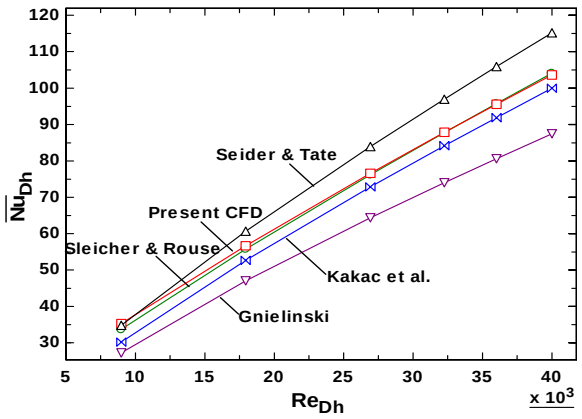

Fig. 2: Variation of average Nusselt number with Reynolds number with uniform wall heat flux

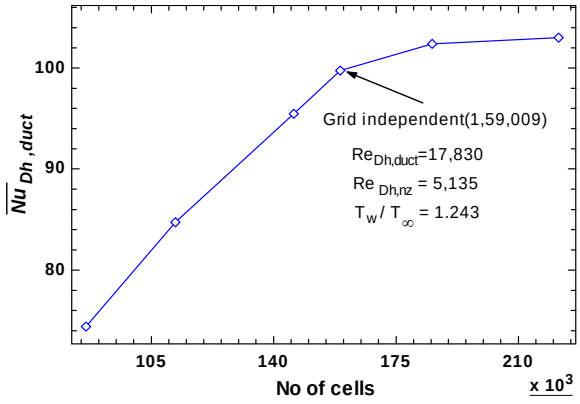

Fig. 3: Effect of number of cells on area weighted average Nusselt number ($\overline{Nu}_{Dh,duct}$)

4. RESULTS AND DISCUSSIONS

4.1. Grid Sensivity Test (conducting triangular potrusion)

A grid sensitivity test for the present numerical investigation from a ribbbed surface in presence of a cross flow jet is shown in Fig. 3. Initially, the area weighted average Nusseit number $\overline{Nu}_{Dh,duct}$ has been increased at a faster rate on coarsening the grids by incorporating more number of cells. It is quite evident from the fig. 3 that the Nussle number has been increased by 34.05% by increasing number of cells from 86,334 to 1, 59,009. A small improvement (i.e., 0.03%) has been noticed as the numbers of cells are increased from 159,009 to 2, 49,549. Thus, the Nusselt number for the computational domain with 159,009 cells is independent of the number of cells after 159,009 cells. For further numerical computations, a computational domain with above mentioned number of cells has been taken. The calculation procedure for area weighted average Nussle number is given as follows:

The area weighted average Nussult number is defined as:

$$\overline{Nu}_{Dh,duct} = \frac{1}{A}\int Nu_{Dh,duct}\, dA \qquad (15)$$

In Eq. 15, area dA is the wetted area i.e. internal surface area from where heat transfer takes place.

The local Nusselt number is calculated as: $Nu_{Dh,duct} = \frac{h_w D_{h,duct}}{k}$ (16)

Where local heat transfer coefficient $h_w = \frac{q_w}{T_w - T_b} = \frac{k\left(\frac{\partial T}{\partial y}\right)_{y=0}}{T_w - T_b}$

The bulk mean temperature is computed from the local temperature, according to Eq. (17).

$$T_b = \frac{1}{A}\int T dA \quad (17)$$

In Eq. (15) and (16), the hydraulic diameter of the duct has been taken to calculate both the average as well as local Nusselt numbers.

The duct Reynolds number is defined as: $Re_{Dh,duct} = \frac{\rho u_{in} D_h}{\mu}$ (18)

Where, u_{in} is the velocity of air in the duct, and D_h is the hydraulic diameter of the rectangular duct. Similarly, the Reynolds number of nozzle ($Re_{Dh,nz}$) is calculated using the nozzle inlet velocity and hydraulic diameter of the nozzle.

4.2. Effect of nozzle Reynolds number on Nusselt number as a function duct Reynolds number

Fig. 4 illustrates the effect of the nozzle Reynolds number on area weighted average Nusselt number for different values of duct Reynolds number. In same plot the variation of the Nusselt number with duct Reynolds number for a duct without cross flow effect has been shown for the sake of comparison. It is noticed that the heat transfer rate has been increased monotonously with the duct Reynolds number irrespective of cross-flow and non-cross-flow effect. This is attributed to an enhanced momentum and heat transfer between heated surface and the bulk fluid moving over it. At a high duct Reynolds number, a higher turbulence is expected, which in turn strongly mixes the cold and hot fluid (i.e., in the vicinity of the solid wall). Thus, the heat transfer at a higher duct Reynolds number is more than that of a lower duct Reynolds number. It is evident that the Nusselt number has been increased by 72.28%, and 64%, respectively when the duct Reynolds number is increased from 18,263 to 54,784 in the presence of a cross- flow jet. It is interesting to note that the Nussle number at a particular duct Reynolds number (i.e., for example, $Re_{Dh,duct} = 18,263$) has been improved by 31.25% when a cross-flow strategy (i.e., $Re_{Dh,nz} = 6,847$) has been implemented as compared to the non-cross-flow strategy.

Therefore, a cross-flow strategy of cooling a hot substrate could be an effective way of heat dissipation from the devices such as electronic chips.

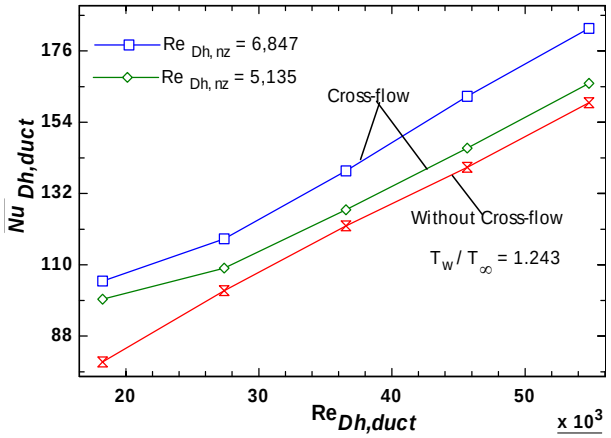

Fig. 4: Variation of the Average Nusslet number with duct Reynolds number ($Re_{Dh,duct}$) as a function of nozzle Reynolds number

The evolution of the turbulent kinetic energy for a cross flow strategy and a non-cross-flow strategy are shown in Fig. 5 (a)-(b). The contour for turbulent kinetic energy in a non-cross-flow strategy has been shown in Fig. 5 (a). Similarly the contour for turbulent kinetic energy for a cross-flow strategy is shown in Fig. 5 (b). It is quite evident that the turbulence level inside the duct is higher than that of the non-cross-flow strategy. Moreover, a stronger recirculation zone is created for a cross-flow case as compared to the non-cross-flow case. The strong recirculation zone helps in bringing more cold fluid from the main stream and effectively mixes with the hot fluid. Therefore, the heat transfer rate with cross-flow strategy is found to be more than that of the non-cross-flow strategy.

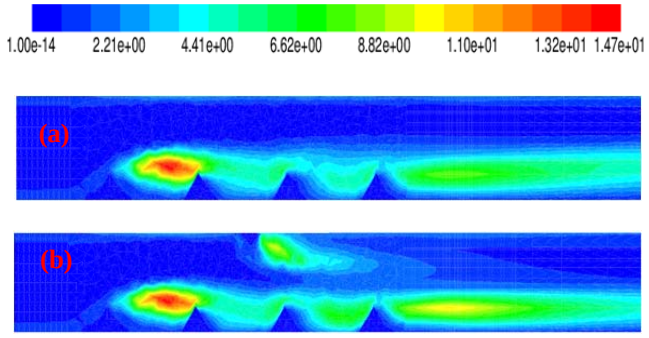

Fig.5: Expanded and cutaway views of turbulent kinetic energy (m^2/s^2) in X-Y plane at $Re_{Dh,duct} = 18,263$ and (a) $Re_{Dh,nz} = 0$ (without cross-flow) (b) $Re_{Dh,nz} = 6,847$ (with cross-flow)

4.3. Effect of different shape of protrusion on heat transfer rate

Two different shape of surface protrusions (i.e., triangular and rectangular shaped) have been deployed for the present investigation. The variation of Nussle number with the geometrical shape of the protrusion for a cross-flow strategy has been depicted in Fig.6. It is observed that the geometrical shape of the protrusions affects the heat transfer rate significantly.

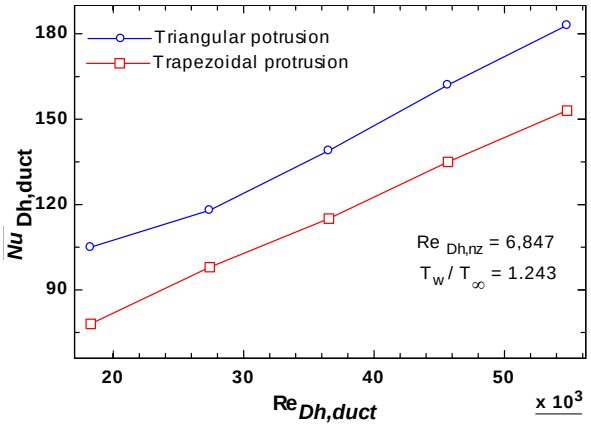

Fig. 6: Average Nusselt number varies with duct Reynolds number for different surface protrusion shape

At a particular duct Reynolds number ($Re_{Dh,duct} = 18,263$), the heat transfer rate is enhanced by 34.6% when trapezoidal protrusions are replaced with the triangular protrusions of same cross sectional area. The flow recirculation in the inter-protrusion gaps is found to be stronger when triangular protrusions are used instead of trapezoidal protrusions. The velocity vectors (i.e., cutaway and expanded views) for triangular and trapezoidal protrusions are shown in Fig. 7(a) and (b) for a constant nozzle Reynolds number ($Re_{Dh,nz} = 6,847$). It is quite clear that the recirculation bubble in the inter-protrusion gaps for triangular protrusions is bigger than the trapezoidal protrusions. The presence of a sharp corner for a triangular protrusion makes a stronger adverse pressure gradient in the inter-protrusion gaps.

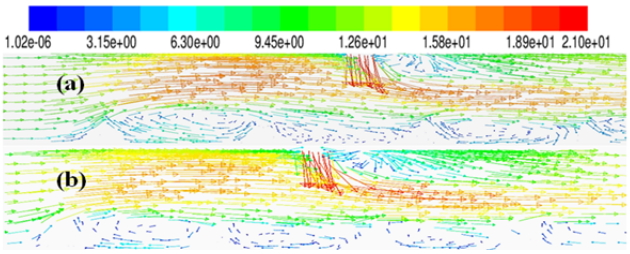

Fig.7 Cutaway views of velocity vectors (m/s) at $Re_{Dh,duct} = 18,263$ and $Re_{Dh,nz} = 6,847$ (a) Triangular (b) Rectangular

This phenomena is, however, not so strong in case of trapezoidal protrusions due to the presence of a flat surface at its top. The strong flow recirculation, in case of triangular protrusions, perhaps brings more cold fluid into the inter-protrusion gaps, and thereby, enhances the heat transfer rate.

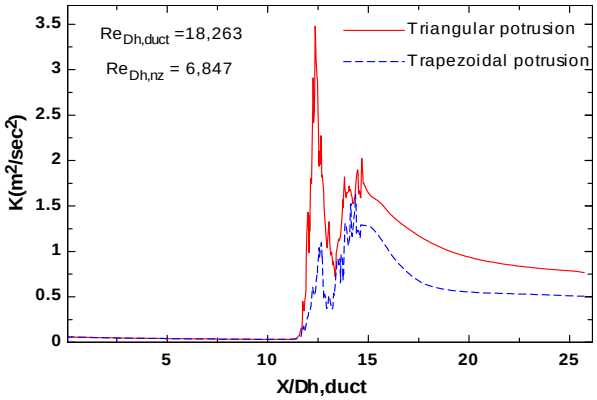

Fig. 8: Variation of duct centreline turbulence kinetic energy at $Re_{Dh,duct} = 18,263$ **and** $Re_{Dh,nz} = 6,847$

Moreover, the turbulent kinetic energy for triangular protrusions is observed to higher than that of a trapezoidal protrusion as has been depicted in Fig. 8. The sudden overshoot of the turbulent kinetic energy is attributed to the presence of surface protrusions. The turbulent kinetic energy is dissipated in the mean flow slowly in the downstream region. Therefore, the turbulent kinetic energy is slowly decreased after having local overshoot.

5. CONCLUSION

Following conclusions are derived from the present investigation:

(i) The heat transfer rate increases with duct as well as the nozzle Reynolds number.
(ii) A higher heat transfer enhancement is obtained for the cross flow arrangement than the non-cross flow arrangement
(iii) The geometry of the protrusions have a significant effect on the heat transfer augmentation
(iv) At a particular duct Reynolds number, the triangular protrusions are found to be better heat transfer augmenter than the trapezoidal protrusions.

6. NOMENCLATURE"

$D_{h,duct}$ Hydraulic diameter of duct (m)

k Turbulent kinetic energy (m^2/s^2)

$\overline{Nu}_{Dh,duct}$ Area weighted average Nusselt number

$Nu_{Dh,duct}$ Local Nusselt number

$Re_{Dh,duct}$ Duct Reynolds number

$Re_{Dh,nz}$ Nozzle Reynolds number

T_{∞} Ambient temperature (K)

T_w Isothermal wall temperature (K)

u_{in} Inlet velocity (m/s)

REFERENCES

[1] Mudawar, I., "Assessment of high-heat-flux thermal management schemes", in: Proceedings of the Seventh Intersociety *Conference on Thermal and Thermo mechanical Phenomena in Electronic Systems*, 1, 2000, pp. 1–20.

[2] Yeh, L. T., "Review of heat transfer technologies in electronic equipment", *ASME J. Electron. Packag.* 117, 1995, pp. 333–339.

[3] Prasad, B.N., and Saini, J.S.," Effect of artificial roughness on heat transfer and friction factor in a solar air heater", *Sol. Energy* 41, 1988, pp. 555-560.

[4] Gupta, D., Solanki, S.C, and Saini, J.S.," Heat and fluid flow in rectangular solar air heater duct having transverse rib roughness on absorber plates", *Sol. Energy* 51, 1993, pp. 31-37.

[5] Lanjewar, A. Bhagoria, J.L., and Sarviya, R.M., "Heat transfer and friction in solar air heater duct with W-shaped rib roughness on absorber plate", *Energy* 36, 2011, pp. 4531-4541.

[6] Ebrahim Momin, A.M., Saini, and Solanki, J. S.,"Heat transfer and friction in solar air heater duct with V-shaped rib roughness on absorber plate", *Int. J. Heat Mass Transf.* 45, 2002, pp. 3383-3396.

[7] Karwa, R. B., and Karwa, K. N., "Experimental study of heat transfer enhancement in an asymmetrically heated rectangular duct with perforated baffles", *Int. Commun. Heat Mass Transf.* 32, 2005, pp. 275-284.

[8] Karwa, R. and Maheshwari, B.K., "Heat transfer and friction in an asymmetrically heated rectangular duct with half and fully perforated baffles at different pitches", *Int. Commun. Heat Mass Transf.* 36, 2009, pp. 264-268.

[9] Bhuiya, M.M.K., Chowdhury, M.S.U., Saha, and Islam M.T., "Heat transfer and friction factor characteristics in turbulent flow through a tube fitted with perforated twisted tape inserts", *Int. Commun. Heat Mass Transf.* 46, 2013, pp. 49-57.

[10] Saini, T. R.P., and Saini, J.S., "Experimental investigation on heat transfer enhancement due to V-shaped perforated blocks in a rectangular duct of solar air heater", *Energy Convers. Manage.* 81, 2014, pp. 374-383.

[11] Zhou, G., Feng, Z., "Experimental investigations of heat transfer enhancement by stagnation region of an impinging plane jet", *Int. J. Heat Mass Transf.* 40, 1997, pp. 3163-3176.

[12] Gardon, R., and Akfirat J.C., "The role of turbulence in determining the heat transfer characteristics of impinging jets", *Int. J. Heat Mass Transf*, 8, 1965, pp. 1261-1272.

[13] Didden, N., Didden, and Ho C.M., "Unsteady separation in a boundary layer produced by an impinging jet", *J. Fluid Mech. 160* 1985, pp. 235-256.

[14] Gauntner, J., Livingoodn N.B, and Hrycak, P., "Survey of Literature on Flow Characteristics of a Single Turbulent Jet Impinging on a Flat Plate", *NASA, TN D*-5652, Lewis Research Centre, USA, 1970.

[15] Tan, L., Zhang, J., and Xu, H. "Jet impingement on a rib-roughened wall inside semi-confined channel", *Int. J. Therm. Sci*. 86, 2014, pp. 210-218.

[16] Xing, Y., Spring, S., and Weigand, B., "Experimental and numerical investigation of impingement heat transfer on a flat and micro-rib roughened plate with different cross flow schemes", *Int. J. Therm. Sci.* 50, 2011, pp. 1293-1307.

[17] Su, L.M., and Chang, S.W., "Detailed heat transfer measurements of impinging jet arrays issued from grooved surfaces", *Int. J. Therm. Sci*. 41, 2002, pp. 823-841.

[18] Wang.L.,Sunden, B., Borg, A., and Abrahamsson, H. "Control of jet impingement heat transfer in cross flow by using a rib", *Int. J. Heat Mass Transf*. 54, 2011, pp. 4157-4166.

[19] Nakabe, K.K., Inaoka, T. Ai, and Suzuki, K,. "Flow visualization of longitudinal vortices induced by an inclined impinging jet in a cross flow for effective cooling of high temperature gas turbine blades", *Energy Convers. Manage*. 38, 1997, pp. 1145-1153.

[20] Menter, F. R., "Two-equation eddy-viscosity turbulence models for engineering applications", *AIAA J*., 32, 1994, pp. 1598–1605.

[21] ANSYS FLUENT Manual User's Guide. Release 12.1. ANSYS, Inc., 2015.

[22] Launder, B.E., Spalding, D.B., "The numerical computation of turbulent flows", *Comp. Meth. Appl. Mech. Eng*. 3, 1974, pp. 269-2879.

[23] Jha, P.K. Dash, S.K., "Employment of different turbulence models to the design of optimum steel flows in a tundish", *Int. J. Numer. Methods Heat Fluid Flow*.14, 2004, pp. 953-979.

[24] Barik, A.K., Dash, S.K., and Guha, A., "Experimental and numerical investigation of air entrainment into an infrared suppression device", *Appl. Therm. Eng*. 75, 2015, pp. 33-44.

[25] Barik, A.K., Dash, S.K., and Guha, A., "New correlation for prediction of air entrainment into an infrared suppression (IRS) device", *Appl. Ocean Res*. 47, 2014, pp. 303-312.

[26] Barik, A.K., Mukherjee, A. and Patro, P., "Heat transfer enhancement from a small rectangular channel with different surface protrusions by a turbulent cross flow jet". *Int. J. of Therm Sci*. 98, 2015, pp. 32-41.

[27] Zuckerman, N. and Lior, N., "Impingement heat transfer: correlations and numerical modeling", *ASME J. Heat Transfer*, 127, 2005, pp. 544-552**.**

[28] Slicher, C.A., and Rouse, M.W., "A convenient correlation for heat transfer to constant and variable property fluids in turbulent pipe flow", *Int. J. Heat Mass Transf*. 18,1975, pp. 677-683.

[29] Sieder, E.N. and Tate, G.E., "Heat transfer and pressure drop of liquids in tubes", *Ind. Eng. Chem*. 28, 1936, pp. 1429-1436.

[30] Kakac, S., Shah, R.K. and Aung, W., "Handbook of Single-phase Convective Heat Transfer", John Wiley and Sons, New York, 1987.